Thermodynamic Entropy: A Natural Metric for Landcover Classification

O. M. Myina [a*] and I. S. Myina [b]

[a] *Department of Chemical Sciences, Taraba State University, Jalingo, Nigeria.*
[b] *Liuham Dynamics Limited, Jimeta-Yola, Nigeria.*

Authors' contributions

This work was carried out in collaboration between both authors. Both authors read and approved the final manuscript.

Original Research Article

ABSTRACT

Most landcover (LC) studies employ physical characteristics involving spectral reflectance. This study employs the concept of energy and entropy for LC classification. Satellite imageries from Landsat-8, the Operational Land Imager (OLI) and the Thermal Infra-Red Sensor (TIRS) captured at 100 m for three years (2013, 2015 and 2017) and resampled to a spatial resolution of 30 m for multispectral measurements were acquired. The normalized difference vegetation index (NDVI) of the study area was computed for both the wet (September/October) and dry (March) seasons of years 2013, 2015 and 2017, respectively; and the vegetation cover maps and landcover classification of the area based on the NDVI values were generated. Land surface temperature (LST) and net radiation of the surface area were computed and used as inputs for computing the surface entropy flux (SEF) of the study area. Overall, the dry season of 2017 had the highest vegetation cover while the wet season vegetation cover was highest in 2015. The high dry season vegetation cover in 2017 is attributable to higher level of living biomass than previous years. NDVI-based LC classification of the area showed an overlap in distinguishing between built-up areas and vegetation cover as well as between bare (land) surface and free water bodies. This is attributable to skewed measure of centrality for the sample distribution possibly resulting from the quality (resolution) of data used or sampling techniques. Free water bodies had the highest SEF values

---

that fall within expected behavior for bodies of such state (liquids). The vegetation covers had the second highest SEF values for the entire site and the highest on land surface, which could be attributed to higher latent heat fluxes of such covers resulting from the evapotranspiration processes. The bare surfaces and built-up area of the study area were observed to have the lowest SEF values. The LC of the study area was reclassified based on SEF values via ground truthing i.e., by taking statistical distribution of well-known surface classes across the years under study. This was successful in distinguishing vegetation cover, surfaces of free water bodies and bare surfaces. A regression analysis revealed that LST influences SEF by up to 69 – 75% while vegetation cover has no appreciable influence on SEF. A two-sample t-test showed a significant (P = 0.05) difference between the SEF for bare surfaces and that for vegetation cover. All these presents SEF as a reliable natural metric for LC classification.

Keywords: Thermodynamic entropy; landcover classification; natural metric; entropy Flux.

1. INTRODUCTION

In very simple terms, thermodynamics is the quantitative treatment of relationships between different forms of energy. In this treatment, the thermodynamic system under study is usually separated from the rest of the *universe* by a boundary, real or imaginary. The nature of the boundary is very critical in this treatment and determines the type of thermodynamic system being considered. A boundary that neither energy nor matter can be transferred to and from its surroundings presents an isolated thermodynamic system. If the boundary is such that energy in form of heat, work and radiation can be transferred to and from its surroundings but not matter, a closed thermodynamic system is in place. When both energy and matter can be transferred to and from the surroundings of a system, such is an open system.

The biosphere in which life exists is made up of the atmosphere, lithosphere and hydrosphere, each having their respective ecosystems. The biosphere, as a thermodynamic system, presents two relatively independent subsystems: subsystem that is responsible for the absorption of incoming solar energy, exergy and exergy conversion into heat flux and informational subsystem that is defined by entropy, information increment and biological productivity [1]. The lithosphere is a complex mixture containing minerals, soil (important for plants and other living organisms), organic compounds, etc. constituting the earth crust. The interface (boundary) between the atmosphere and lithosphere, hydrosphere and lithosphere; and biosphere and lithosphere is the soil (land) surface. This interface is the location of large transformations of energy i.e., energy exchange between the atmosphere and the land (earth) surface. The solar radiation absorbed by the land surface is transformed into sensible heat (heat exchange that results in change of body temperature and other thermal properties without change of state), latent heat or stored in the soil as ground heat with significant implications to the environment [2]. Thus, the solar radiation warms the land surface and provides energy to drive weather and climate; the land surface also contributing to the energy budget of the environment.

By nature of the land surface, the atmosphere, lithosphere, hydrosphere combination is considered an open [1] thermodynamic system. Turbulent mixing of air causes the exchanges of sensible and latent heat between land surface and the atmosphere, which results in heat and moisture conveyance influenced by topography, vegetation, landforms and structure of the environment [3].

One of the key parameters in the study of climate change is land surface temperature (LST), which plays a key role in the interaction between atmosphere and land (lithosphere). It is influenced by a combination of natural and anthropogenic factors like altitude, precipitation, ground moisture, landcover type, urbanization and use. LST is a major factor that controls most physical, chemical and biological processes in the biosphere and has an inverse relationship to vegetation [4]. When the land surface is impacted with energy exchange and temperature changes, not only are ground thermal properties dynamic, but superimposed on these complex relationships are annual and diurnal patterns of solar radiation, including irregularities in weather patterns [5].

In the Sudano-Sahelian region for instance, considerable land surface changes occur annually. The predominance of annual grasses

makes the land surface vary from bare during the dry season to luxuriant vegetation during the rainy season [6]. Therefore, measurements of the magnitude and variability of surface sensible, latent and specific (ground) heat fluxes (the sum of which is the total energy flux i.e., net radiation) becomes important because of the significance of local processes and the kind and intensity of weather experienced in a region [3]. The kind and intensity of weather impacts sustainable agriculture.

Entropy, denoted *S*, is a thermodynamic state quantity that measures the degree of randomness or disorder of the molecules (constituents) of a system. For a reversible change taking place at a fixed temperature (*T*), the change in entropy (∆*S*) is equal to the heat energy absorbed or evolved (*q*) divided by the temperature,

$$\Delta S = \frac{q}{T} \qquad (1)$$

Positive ∆*S* value implies heat is absorbed and corresponds to increase in entropy while a negative value shows heat is evolved and entropy decreases. Equation (1) is generally referred to as the Second Law of Thermodynamics, according to which non-stationary nonequilibrium processes that are far from thermodynamic equilibrium, adapt to stable states in which they dissipate energy and produce entropy at the maximum possible level [1].

Entropy can be used to form a framework in studying the environment, understanding and identifying regions that indicate an inefficient use of the energy radiated to land surface from the sun. An efficient utilization of this energy (resulting in low entropy) would imply a healthy environment that supports sustainable agriculture, whereas high entropy would suffice as a warning to impending or occurring environmental degradation. The use of entropy to prioritize which impacts to avoid and which to mitigate/remediate, as well as approaches to climate change, seems rational. This research, therefore, aims at using surface entropy flux (SEF) techniques to determine landcover classes of the study area.

2. MATERIALS AND METHODS

2.1 Research Design

Largely, landcover (LC) studies employ physical characteristics involving spectral reflectance.

This study applies the concept of energy and entropy for LC classification. The general framework of the research involved the acquisition of data, primarily, satellite imageries for a period of three years: 2013, 2015 and 2017. These years were chosen because they had the most complete and valid corresponding climatic data from the local weather station. The data used for the research was acquired from Landsat-8, the Operational Land Imager (OLI) and the Thermal Infra-Red Sensor (TIRS) which is captured at 100 m but resampled to a spatial resolution of 30 m for multispectral measurements [7]. The spectral structure of the reflected radiation in comparison with the structure of the incoming solar radiation per every elemental area (pixel, element of thermostatic system) allows estimation of the thermodynamic parameters of ecosystems at the moment of measurements [1]. The required images were from the month of March (which had the minimal cloud cover and were captured at the time when the region experienced high temperatures to represent the dry season) and September/October (to represent the wet season). September/October were selected because they are months with minimal cloud cover during the wet season in the study area. The satellite images were downloaded from the archives of the United State Geological Survey (USGS).

The acquired data was preprocessed, using the DOS1 (Dark object Subtraction 1) technique, to correct for the influence of top-of-atmosphere interference. DOS 1 is an image-based method [8] for converting Landsat images from digital number (DN) to surface reflectance without requiring any information about atmospheric conditions. The net radiation and land surface temperature (LST) were computed from the acquired data and used to compute the SEF of the area.

2.2 Study Area

The study area (Fig. 1) was chosen for its proximity and as one with all the major land surfaces like free water, vegetation, rock outcrop and grassy farmlands; hence suitable for testing of a parameter as a classification metric. Also, given that LC and land use (LU) composition strongly influences future development potential in terms of sustainability and economy [9], the rapid suburbanization of the study area resulting from the siting of a Federal University beside it, makes its choice essential and needful. It is

bordered by the following coordinates, 09.500^o N, 12.400^o E at the upper left corner and 09.300^o N, 12.6500^o E, at the bottom right corner and encompasses the following villages; Galrole, Langire, Wuro Medi, Wuro Dole, Wuro Mbonara, Gokra, Dagri, Kofare and Girei. The area falls between the northern Guinea Savannah vegetative zone, characterized by high grasslands with shrubs and fewer trees. Common grasses in this region include; *Cassia* species, *Chlorispilosa*, *Tridax precumbe*, *Euphopia* species, *Leucas martiniesis*, *Eroggrostremulla*, *Pennisetum* sepcies and common trees such as the *Viteelara paradoxa*, *Tamarindus indica*, *Tamalinia* species, *Accasialbida* and *Adosomnia digitata*. Human activities such as cultivation for many years, have changed the ecosystem and characteristic features of the area to a dry Sudan Savannah. Common crops grown are maize, groundnut, cowpea and sorghum. The area is trademarked with gently sloping terrain to steeply sloped region of the Bagalle hills. These hills are in the south-east quadrant, occupying the entire quadrant. Rock outcrops and/or rocky surfaces appear at the south-west quadrant and extend near the banks of the River Benue.

2.3 Geology and Soils of the Study Area

Settlements of Wuro Medi, Darware, Langire to Gogra are suitated on sandy loam to sandy clay soils, with no or few iron concretions, mostly over sandstones. The Dagri and Kaffare settlements are situated on rock outcrops and have shallow skeletal soil on Bima sandstone ridges with sandy loam soil in the valleys. The Girei settlement is situated on shallow skeletal soil over granite, basalt, sandstone and ironstone. The soils appear yellowish brown in color, and are poorly drained due to the prevalence of mottling in the horizon. The river Benue is situated in sandy, loamy and clayey soils of alluvial areas. The soil's pH is acidic (range of 6.5 – 6.9), cation exchange capacity (CEC) is low in organic carbon, total nitrogen and available phosphorus.

2.4 Developing Vegetation Index Map

Vegetation indices are mathematical transformations, usually ratios or linear combinations of reflectance measurements in different spectral bands (or channels), particularly the visible and near infrared bands. In developing the vegetation index map, the NDVI of the study area was computed via equation (2)

for both the wet and dry season of the years 2013, 2015 and 2017 using data from the Landsat-8 (OLI/TIRS) satellite; the red and near infrared bands being the bands of interest [10].

$$NDVI = \frac{R_{NIR} - R_R}{R_{NIR} + R_R} \qquad (2)$$

where R_{NIR} and R_R = reflectance in the near infrared and red bands, respectively.

2.5 Land Surface Temperature

The approach already reported [3,11] was adopted in computing LST from the Landsat-8 TIRS data. The emissivity (rate of emission of heat from the surface of a heated body) of the land surface of the study area was computed (equations 3 and 4) from the NDVI [8] of the wet and dry seasons of the years under study for use in generating a land surface temperature map of the study area as an input for estimating SEF. The thermal infrared band of the Landsat 8 level 1 product acquired with a resampled spectral resolution of 30 m [7] was converted to radiance and to brightness temperature. The brightness temperature and emissivity raster were then used as inputs in computing the land surface temperature (in Kelvin) of the study area.

$$\varepsilon = f_v \varepsilon_v + (1 - f_v)\varepsilon_v \qquad (3)$$

given that

$$f_v = 1 - \left[\frac{NDVI_{max.} - NDVI_i}{NDVI_{max.} - NDVI_{min.}}\right]\alpha \qquad (4)$$

where ε = emissivity, α = function of leaf orientation distribution canopy, $NDVI_{max.}$ is the NDVI value for maximum (complete) landcover, $NDVI_{min.}$ is the NDVI value for study area and $NDVI_i$ is the NDVI value for point (location) *i*.

2.6 Conversion of Digital Number to Radiance

Digital numbers (DN) were converted [4] to radiance using equation (5).

$$L_\gamma = \left[\frac{L_{max.} - L_{min.}}{255}\right] \times DN \times Bias \qquad (5)$$

where L_γ is the spectral radiance at the sensor.

2.7 Conversion of Radiance to Brightness Temperature

The Planck's inversion function (equation 6) was applied in converting the radiance value to brightness temperature.

$$T = \frac{K_b}{\ln[(K_a/R_v) + 1]} \qquad (6)$$

where T is brightness temperature (in Kelvin), K_a and K_b (1331 and 775, respectively) are calibrated thermal constants 1 and 2, and R_v is the cell radiance value.

2.8 Conversion of Brightness to Land Surface Temperature

The already developed model [10,12] for compensation of spectral surface emissivity and vegetation cover in the derivation of land surface temperature was employed in converting from brightness temperature to land surface temperature (equation 7) based on Agone and Bhamare approach [13].

$$LST = \frac{T}{1 + (\lambda kT/hc) \ln \varepsilon} \qquad (7)$$

or

$$LST = \frac{T}{1 + \lambda \kappa \ln \varepsilon} \qquad (8)$$

where LST is the land surface temperature (K), T is the brightness temperature (K), λ is the wavelength of emitted radiance (10.8 μm), k is Boltzmann constant, h is Plank's constant, c is velocity of light, ε is emissivity and $\kappa = k/hc = 14395$ μm.

2.9 Computing Surface Energy Flux

The net radiation (i.e., the energy that is available to influence the local environment) for the study area was computed at the time of satellite overpass using the SEBAL model [14] as defined and simplified [2,15]:

$$R_n = (1 - \alpha)R_{dsr} + \varepsilon R_{dlr} - \varepsilon \sigma T_o^4 \qquad (9)$$

where R_n is the net radiation in Wm^{-2}, α is the albedo, ε is the emissivity of the surface, σ is the Stefan-Boltzmann constant, T is the land surface temperature, R_{dsr} is the downward shortwave radiation and R_{dlr} is the downward longwave radiation.

2.10 Computing Surface Entropy Flux

SEF was computed, in line with equation (1), as the ratio of net radiation approximation at the time of satellite overpass and the land surface temperature. Net radiation (Wm^{-2}) is an energy flux depicted as sum of sensible, latent and ground heat fluxes [16]. Since the energy flux is measured at the time of satellite overpass, $\Delta t \cong 1$ and Wm^{-2} = Jm^{-2}. The energy budget equation defines the net radiation as,

$$R_n = H + G_{et} - U_s \qquad (10)$$

where H is sensible heat, G_{et} is latent heat of evapotranspiration and U_s is the energy utilized in heating the soil. Thus, q (equation 1) is equal to R_n, T equals LST and analogous of equation (1) becomes,

$$SEF = \frac{R_n}{LST} \qquad (11)$$

2.11 Entropy Flux and Biophysical Properties

A regression analysis was conducted to determine the relationship between NDVI and SEF, and between LST and SEF. The SEF values for water bodies, built areas and vegetation cover were randomly sampled and tabulated for comparison. Similarly, SEF values for the various landcover classes in the study area were randomly sampled and tabulated for comparison.

3. RESULTS AND DISCUSSION

3.1 Climatic Conditions of Study Area

The climatic conditions of the area are fairly constant. Temperature is high during most parts of the year because of the radiation influx which is relatively high and distributed throughout the year. The highest maximum temperature of 49.73 °C and minimum temperature of 7.75 °C (Table 1) was recorded during the period of 2013 through to 2017. The average temperature recorded for the period of the observation was 38.32 °C. The monthly average revealed that the lowest ambient temperature (24.5±4.5 °C) are in August while the highest (about 44 °C) was recorded in March (Fig. 2).

The rainfall is the most variable element with the highest precipitation of 99.19 mm. The average observed was 2.09 mm. The rainfall starts in April and ends in October with August having the highest precipitation (Fig. 3). The maximum relative humidity of 0.9 fractions, with an average of 0.47 fractions was observed. The highest relative humidity (about 0.82 fractions) was also observed in August like precipitation (Fig. 3). The observed precipitation and the relative humidity agree with reported findings [17]. The maximum wind speed of 3.25 m/s was observed with an average of 1.55 m/s. Monthly average show that the wind speed is high at the onset of the wet season (Fig. 3). The solar radiation flux for the region is relatively high. Maximum solar radiation observed was 27.99 MJ/m^2 (22.31 MJ/m^2 average) and tends to be distributed during most parts of the year (Fig. 2).

The soil of the region is characterized as sandy loam underlain by sand to silt clay. The soil appears yellowish-brown and is poorly drained due to the prevalence of mottling in the horizon (Table 2). The soil's pH (6.5 – 6.9) is acidic with CEC low in organic carbon, total nitrogen and available phosphorus.

3.2 Normalized Difference Vegetation Index (NDVI)

Table 3 presents the NDVI-based landcover classification for the study area. It shows an overlap in distinguishing between built-up areas and vegetation cover on one hand, and bare surface and water surface on the other; as a result of reasons alluded earlier. The computed NDVI for the study area (Tables 4 & 5) show average values of 0.1996, 0.2443, and 0.3322 for the dry season (i.e., March) for years 2013, 2015 and 2017 while that of the wet season (i.e.,

September/October) for the same years were 0.5786, 0.6019 and 0.5196 respectively. The dry season of 2013 showed the lowest NDVI value. This suggests the volume of water bodies was higher (and deeper) than the same month in other years. Same was observed in the wet season for year 2015. In general, the quality and density of vegetation [4,18,19] cover for the study area on an average, was higher in 2015 and 2017 for the wet and dry seasons, respectively.

The dry season (March) vegetation maps generated show that most parts of the study area were bare (i.e., no significant vegetation cover) in March of 2013, with patches of vegetation covering parts of the Bagale hills (lower right quadrant of map) and extending into Girei, Wuro Dole and Wuro Medi settlements. Granular patches of vegetation cover were observed between Galrole and Langire villages, extending more towards Galrole than Langire village. Patchy vegetation is also observed around Kaffare village, extending left ward (i.e., the bottom left quadrant of the map) just above the River Benue. This vegetation cover above the river is situated on lands that get fed with water from the river (Fig. 4). This pattern of vegetation cover distribution changed in the dry season of 2015 but the bare nature of the land remained. Patches of vegetation cover were observed bordering the settlements around the Modibbo Adama University of Technology (MAUTECH), Yola, towards the upper left and bottom right. The vegetation cover around the Bagale hills were patchy and sparing at the top of the hills (i.e., in the bottom right corner of the map). Vegetation cover was also observed around the Wuro Dole village and between Galrole and Langire villages as well as to the left of Kaffere village (Fig. 5)

Table 1. Statistical Summary of observed weather conditions of study area, 2013 – 2017

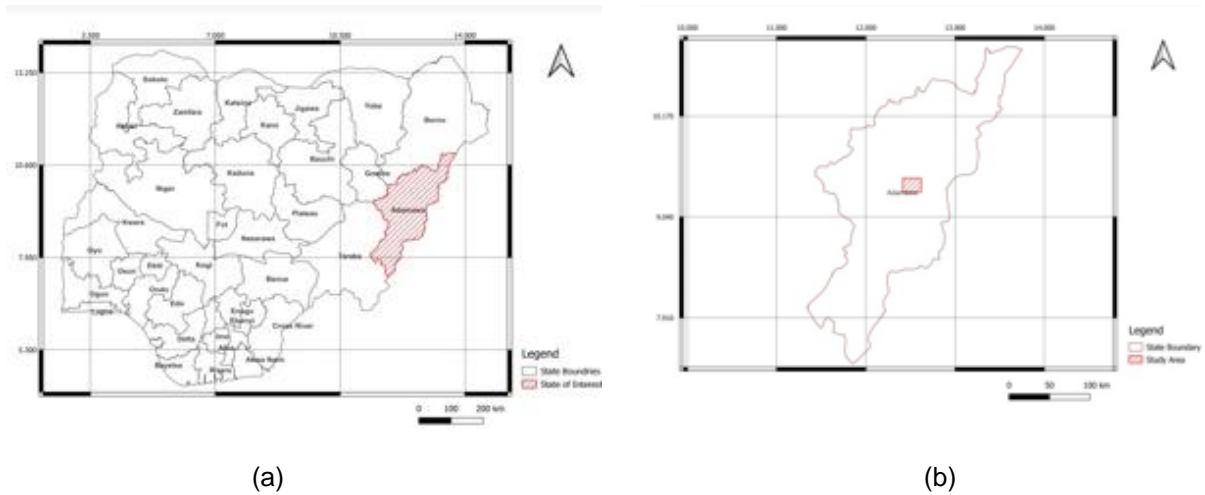|	Maximum Temperature (°C)	Minimum Temperature (°C)	Precipitation (mm)	Wind Speed (m/s)	Relative Humidity (frac.)	Solar Radiation (MJ/m²)
Minimum	24.32	7.75	0.00	0.65	0.09	2.53
1st Quantile	34.86	16.64	0.00	1.29	0.28	21.50
Median	38.77	21.34	0.00	1.51	0.45	23.20
Mean	38.32	20.02	2.09	1.55	0.47	22.31
3rd Quantile	41.97	23.43	0.93	1.78	0.66	25.18
Maximum	49.73	28.34	99.19	3.25	0.93	27.99

(a) (b)

Fig. 1. Map of Nigeria (a) showing state (Adamawa State) where study area is located and Map of Adamawa State (b) showing location of study area
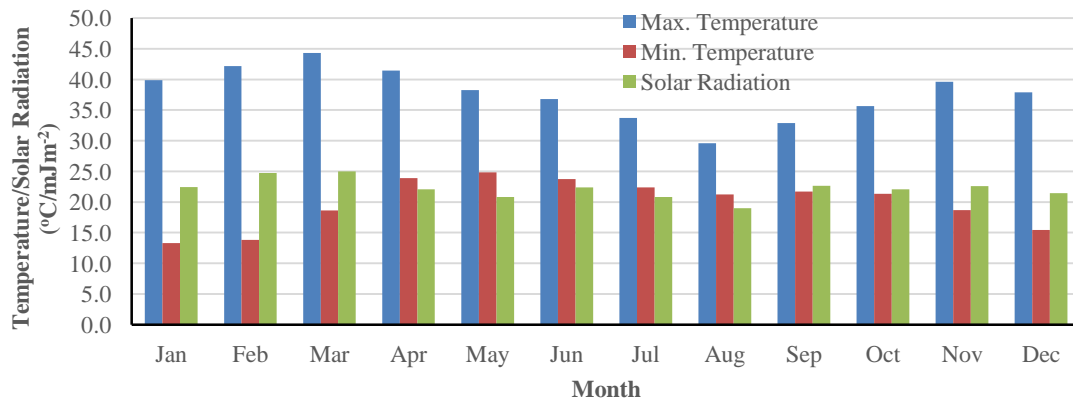

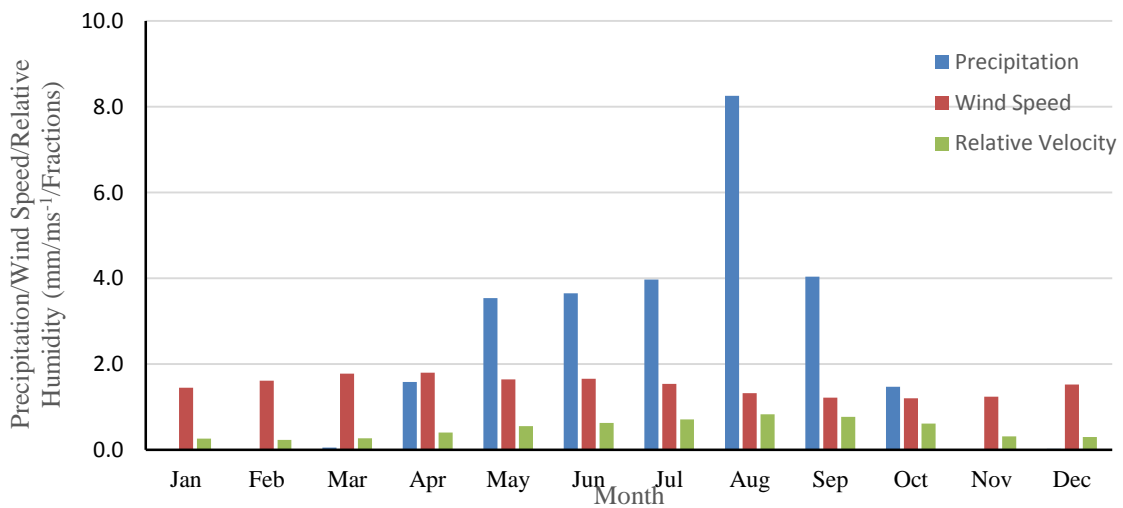**Fig. 2. Monthly averages of temperature (Minimum and Maximum) and solar radiation**

Fig. 3. Monthly averages of precipitation, wind speed and relative humidity

Table 2. Listing of five classes of soils in the study area

Label	Name	Description
FC	Concretionary Leached Ferruginous Tropical Soils	Sandy loam to sandy clay loam with concretionary iron-pan over granite or sandstone
RWE	Rock outcrops, Raw Mineral Soils and Weakly Developed Soils of erosion	Shallow, skeletal soils over granite, basalt, sandstone and ironstone
FL	Leached Ferruginous Tropical Soils, without iron concentrations	Sandy loam to sandy clay soils, with no or few iron concretions, mostly over sandstone
R-FL	Sandy loam to sandy clay soils, with no or few iron concretions, mostly over sandstone	Rock outcrops and shallow skeletal soils on Bima Sandstone ridges and sandy loam in valley
YWD	Weakly Developed Soils of deposition and Hydromorphic Soils	Sandy, loamy and clayey soils of alluvial areas

Table 3. NDVI-based landcover classes

NDVI Range	Class Name
0.0001 – 0.2814	Bare Surface
0.2815 – 1.0000	Vegetation
-1.0000 – 0.0000	Others (mostly Free Water Surface)

Table 4. The NDVI values for dry season (March) of 2013, 2015 and 2017

	2013	2015	2017
Maximum	0.6015	0.3986	0.7315
Mean	0.1996±0.0530	0.2443±0.0170	0.3322±0.0457
Minimum	-0.4465	0.1496	0.0991

Table 5. The NDVI values for wet season (September/October) of 2013, 2015 and 2017

	2013	2015	2017
Maximum	0.8484	0.8844	0.7837
Mean	0.5786±0.1204	0.6019±0.1454	0.5196±0.0991
Minimum	0.3088	-0.5926	-0.2124

The vegetation cover map of March 2017 was observed to differ significantly to that of the previous years (2013 and 2015). A greater portion of the study area was covered with vegetation and only significantly larger settlements reflected no vegetation cover, particularly regions around Kaffere and Girei settlements. A trail of bare surfaces from Wuro Dole through Girei to Gogra is observed from the map (Fig. 6). These are portions of the stream that runs from the Bagale hills through Girei downwards.

Overall, it was observed that the dry season (March) of 2017 had the highest vegetation cover with almost the entire map surface of the study area covered with vegetation. This could be attributed to higher levels of living biomass than

the previous years [20], resulting to the high NDVI values observed (Table 4). The water bodies were also observed to appear as bare surface rather than water. This is due to the fact that the NDVI values for water are usually below zero unlike the minimum (0.0991) observed [21]. Also, the resolution of the acquired image may aggregate portions of narrow waterways with nearby lands; thus, recording such aggregated values as lesser than expected. In the dry season of 2013, a large surface of the study area was covered with vegetation and the water body was properly represented. However, in the same season of 2015, there was a drop in the vegetation cover, most especially around the Bagale hills extension. Vegetation cover around the Kaffare settlements appeared statistically (P = 0.05) consistent between the dry seasons of

2013 and 2015. The wet season (September/October) of years 2013, 2015 and 2017 were observed to generally have high NDVI values with maximum values ranging from 0.7837 to about 0.8844 (Table 5) reflecting a higher density of living biomass [22] consequent upon high levels of precipitation. Surfaces around settlements like Girei and MAUTECH, Yola, were marked as patches of bare land. The stream path, running from the Wuro Dole village through Girei to Gogra village, was also marked as bare surface.

3.3 Surface Entropy Flux (SEF)

The entropy flux at the surface of free water bodies (e.g., River Benue) yielded the highest SEF values in the study area. This is so because bulk of the solar energy reaching such surfaces is used for evaporation (change the state of such bodies) and the remaining fraction is used to heat the surrounding air. Since no significant portion of the energy is absorbed, the net radiation (R_n) observed is high. In using up the energy for evaporation (G_{et}) and heating of the surrounding air (*H*), little or no energy is left to

increase the temperature gradient between the surface and deeper parts of such bodies. Thus, no downward flow of energy and no significant increase in temperature of such bodies. Given that entropy is seemly a measure of how energy is dissipated, the dissipation of energy at the surface of free water bodies is higher with consequent higher SEF values. Land surface covered by vegetation had the next high values for SEF given the inverse relationship between vegetation and LST [4]. The observed LST in regions of the study area with significant vegetation cover was low, since energy reaching such surfaces is used by the vegetation (and induces transpiration) but never absorbed by the soil ($U_s = 0$) due to canopy effect and sometimes mulching. The resultant energy (G_{et}) dissipated is significantly high with attendant low surface temperature and high SEF. Although, SEF over vegetated surfaces would always be lower than those observed over free water body surfaces; exceptions exit for regions (or periods) with very high relative humidity. In such regions, the SEF values for vegetated surfaces may appear same with those observed over free water body surfaces.
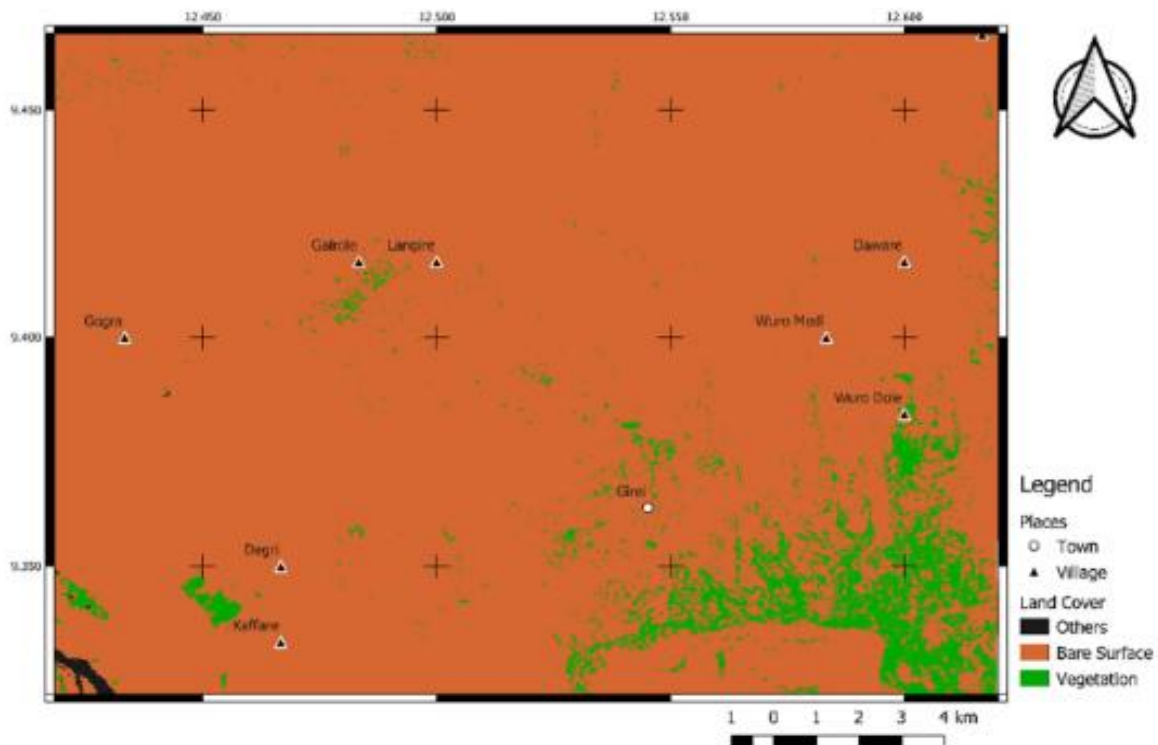

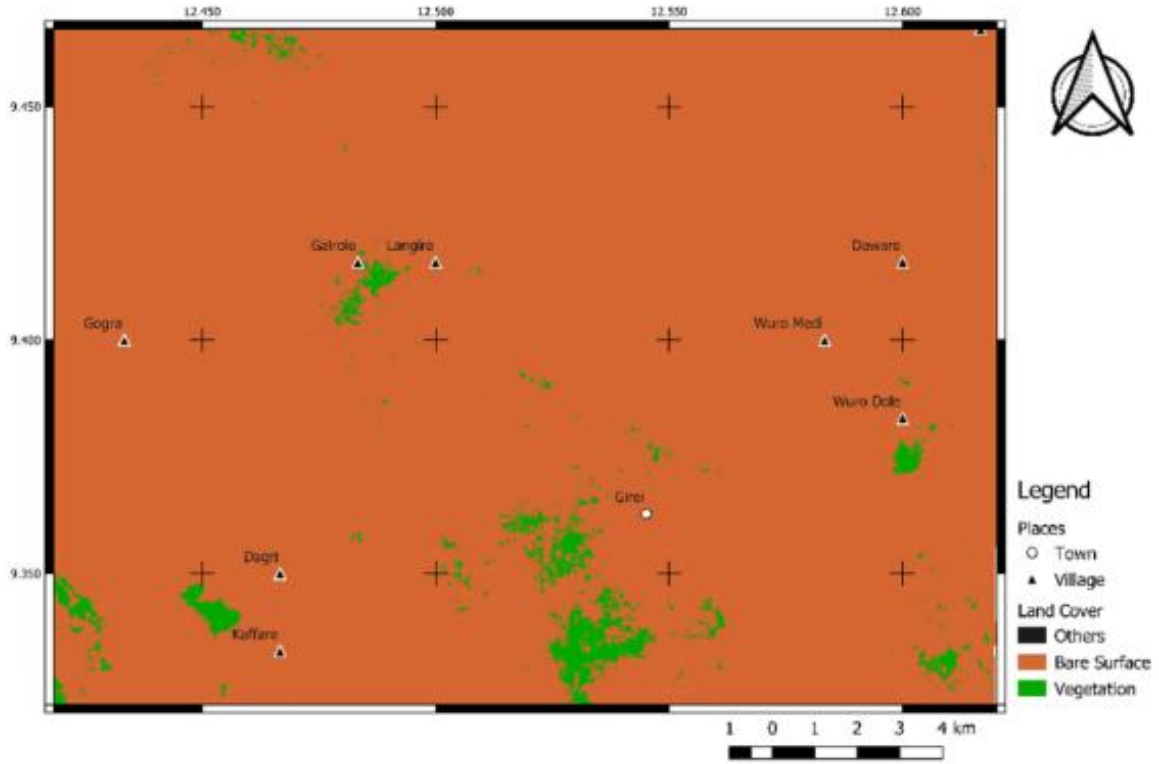**Fig. 4. Vegetation cover map of study area for dry season (March) of 2013**

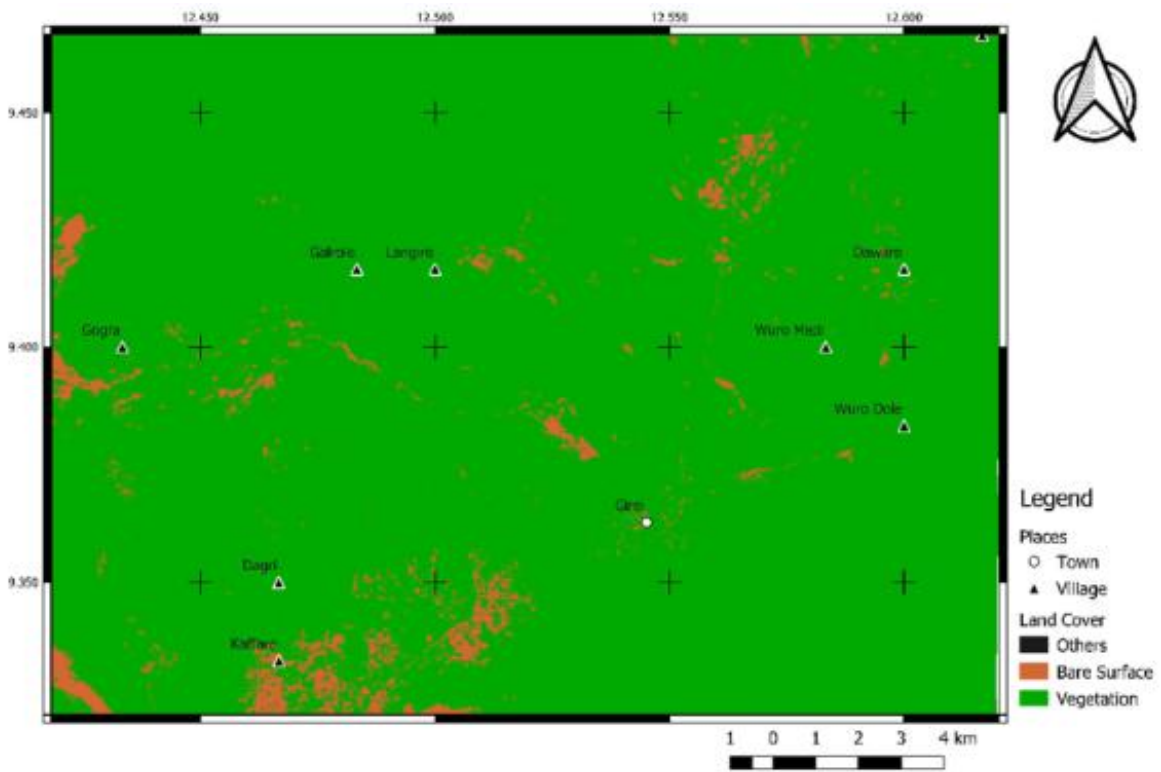**Fig. 5. Vegetation cover map of study area for dry season (March) of 2015**

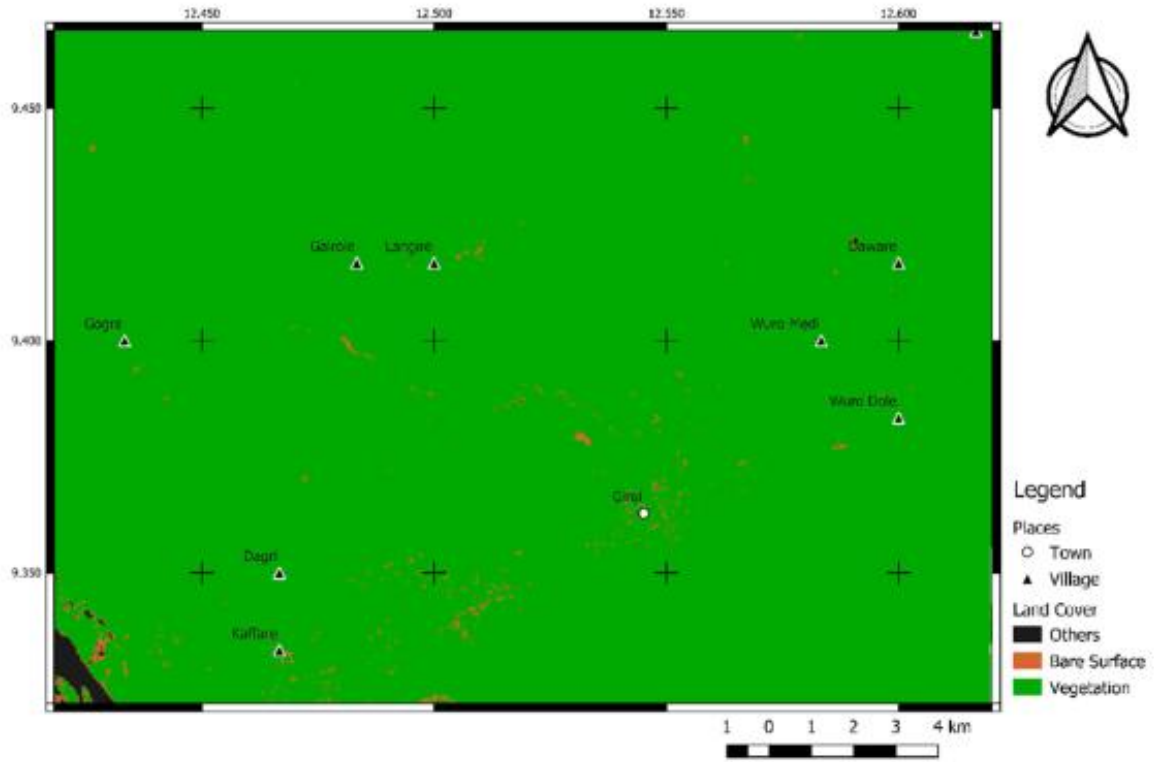**Fig. 6. Vegetation cover map of study area for dry season (March) of 2017**

Fig. 7. Vegetation cover map of study area for wet season (September) of 2013
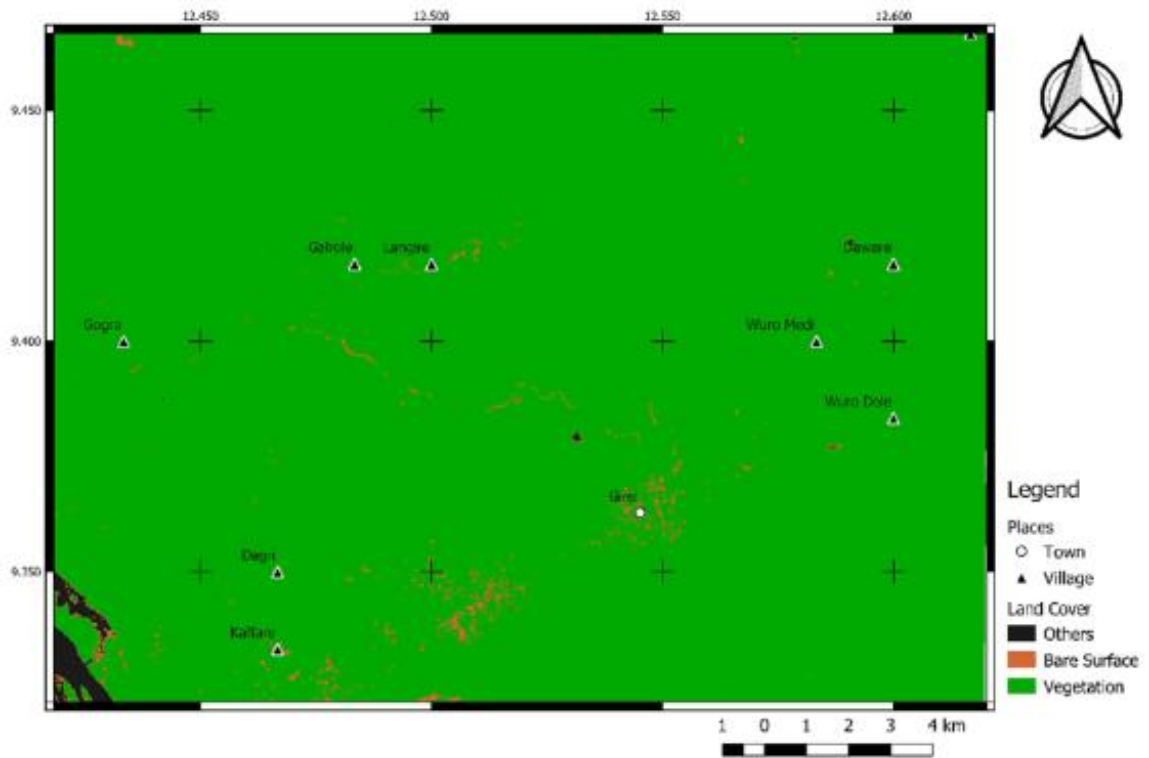

Fig. 8. Vegetation cover map of study area for wet season (September) of 2015
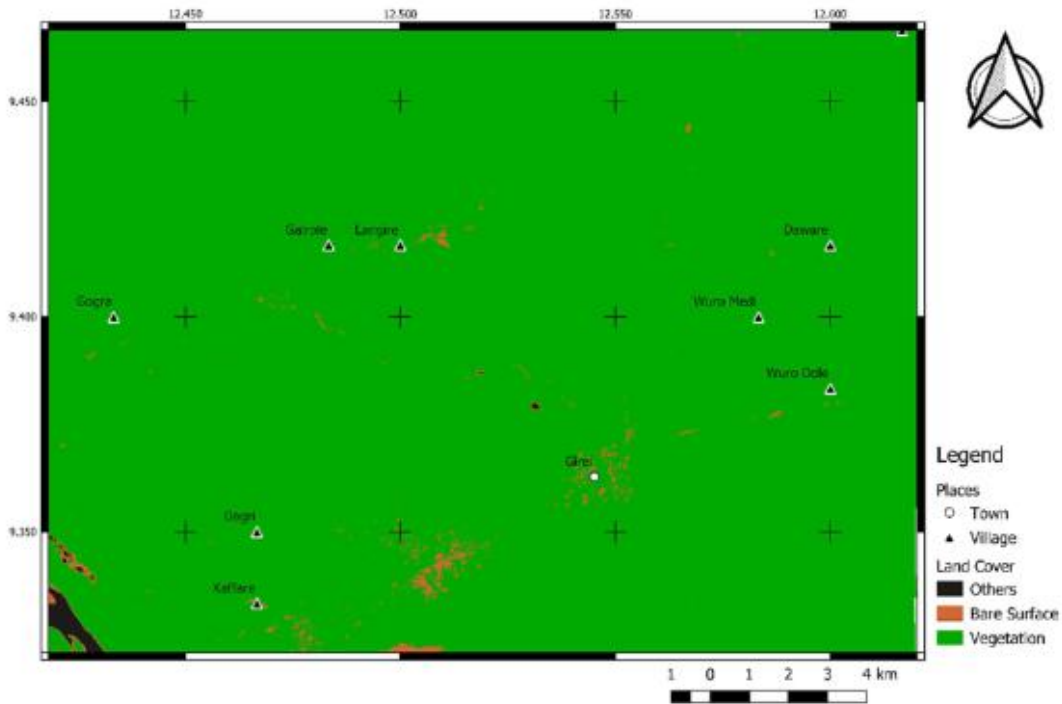
Fig. 9. Vegetation cover map of study area for wet season (September) of 2017

Table 6. Dry season (March) surface entropy fluxes of study area in Jm^{-2}K^{-1}

	2013	2015	2017
Maximum	2.861	3.060	2.747
Mean	2.380 ± 0.067	2.592 ± 0.102	2.364±0.0599
Minimum	2.102	2.418	1.990

Bare surfaces and built-up regions of the study area were observed to have the lowest SEF values. This is expected (equation 10) since a large portion of the net radiation reaching such surfaces is absorbed as ground heat, making the negative U_s larger and R_n smaller, and resulting in lower SEF. However, when such surfaces are moist or wet, a larger portion of the R_n is used in G_{et}, which significantly reduces the surface temperature until evaporation is no longer possible. The increase in G_{et} increases the R_n and results to larger SEF values. This suggests that, though the SEF values of bare surfaces are lowest, surfaces that can absorb moisture would yield higher SEF values than dry surfaces. Year 2017 had the lowest SEF value while 2015 had the highest value (Table 6).

The wet season (September/October) of years 2013 and 2017 showed almost same lower average SEF values of 2.587 and 2.563 Jm^{-2}K^{-1} respectively, while the highest average SEF value of 2.633 Jm^{-2}K^{-1} was recorded in 2015.

The surface entropy flux map of the study area for the dry season (March) of 2013 reveal the highest SEF values on water surface (i.e., River Benue) at the bottom left corner of map while the Bagale hill and strips to the left of Kaffare village had higher SEF values than most surfaces of the study area. Settlements like Girei, Wuro Dole and Daware had moderately low SEF values (Fig. 10). The dry season of 2015 presented a different pattern. The highest SEF value was recorded around the Bagale hills. Girei and Wuro Dole settlements also had higher SEF values than other regions of the study area.

The dry season (March) of 2017 was observed to have the highest SEF values around regions above the Gogra village. River Benue was also one of the surfaces with the highest SEF values. The Bagale hills were observed to have high SEF values but not as high as those for River Benue. Settlements like Daware and Girei (the entire right side of the map) presented as regions

of the study area with average SEF values with some patches of moderately high SEF values (Fig. 12).

The SEF maps for the dry season of 2013 and 2015 revealed that water bodies tend to have the highest SEF values than land surfaces or vegetation cover. This is expected since the entropy (level of disorder) of such bodies (liquids) are higher than solid bodies [22] and in line with the 2nd law of thermodynamics.

The SEF values for vegetation covers were observed to be higher than values for regions with bare surface (no vegetation cover). This is consistent with reported observations [23] in quantification of thermodynamic entropy budget of land surfaces. They observed that latent heat flux (G_{et}) caused the largest entropy transfer and it approximately doubled those of sensible (*H*) and ground heat (U_s) flux. Therefore, entropy transfer increases with vegetation. Thus, vegetation has a significant role in increasing the entropy production by altering the absorption of solar radiation and decreasing the surface temperature. The role of vegetation in decreasing

land surface temperature has also been reported [4].

SEF map of the study area in the wet season (September) of 2013 presents high SEF values along the upper boundary while most of the settlements had low SEF values. Villages like Wuro Dole, Wuro Medi, Langire, Galrole, Gogra and Kaffare all showed low SEF values. River Benue has the highest SEF value (Fig. 13). The year 2015 map for wet season presents River Benue surface and the bowl of Langire, Wuro Medi and Daware settlements with the highest SEF values. Settlements on the diagonal of Kaffare and Girei have lower SEF values (Fig. 14). The wet season (October) of 2017 recorded its highest SEF values on the River Benue and regions of the Bagale hills extension. A larger portion of the study area was observed to have average to slightly high SEF values (Fig. 15). Generally, therefore, the generated SEF maps for the wet season had larger portions of the study area covered by above-average SEF values, typically, due to the latent heat flux as a result of vegetation and high soil moisture [23,24].
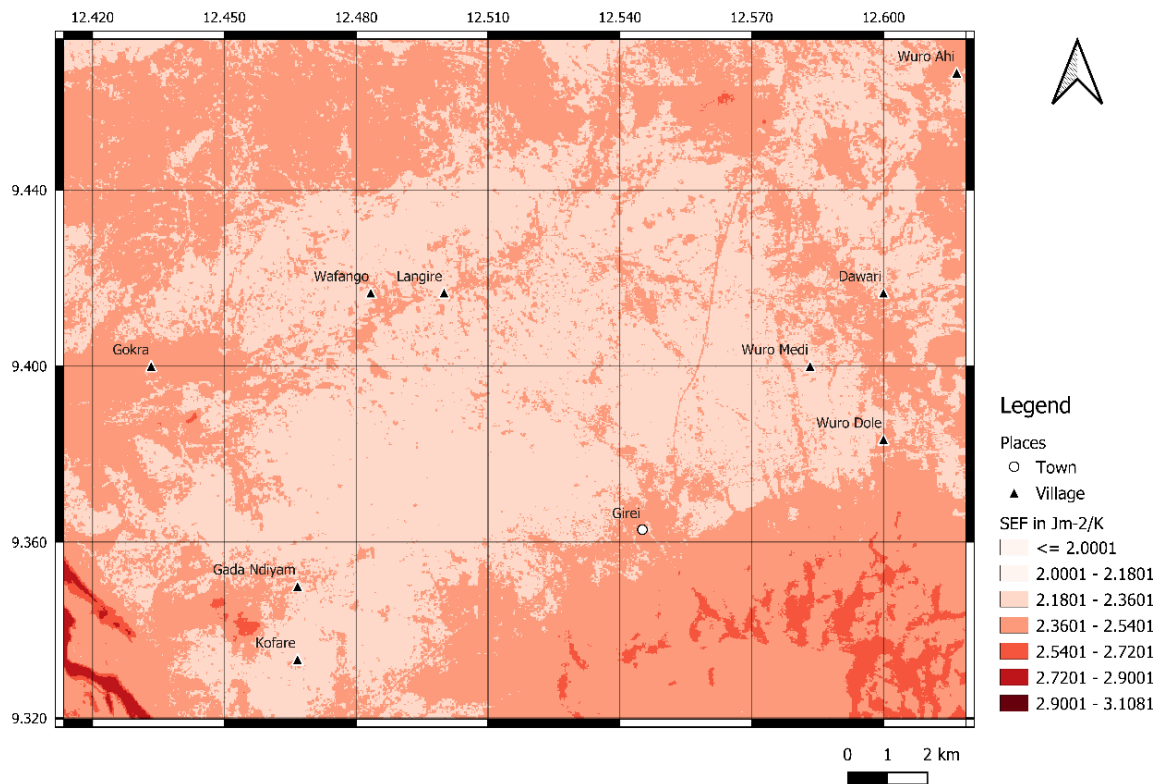

Fig. 10. Dry deason (March) 2013 surface entropy flux map of study area (Jm^{-2}K^{-1})

Table 7. Wet season (March) surface entropy fluxes of study area in Jm^{-2}K^{-1}

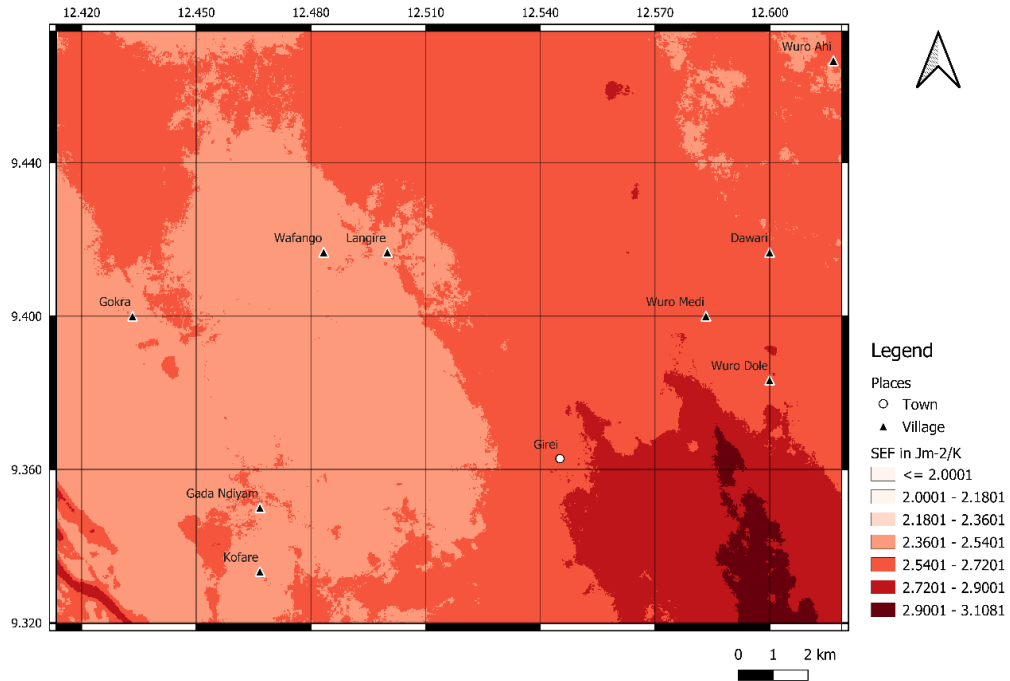|	2013	2015	2017
Maximum	2.874	2.887	2.822
Mean	2.587 ± 0.073	2.633 ± 0.053	2.563 ± 0.067
Minimum	2.230	2.034	2.130

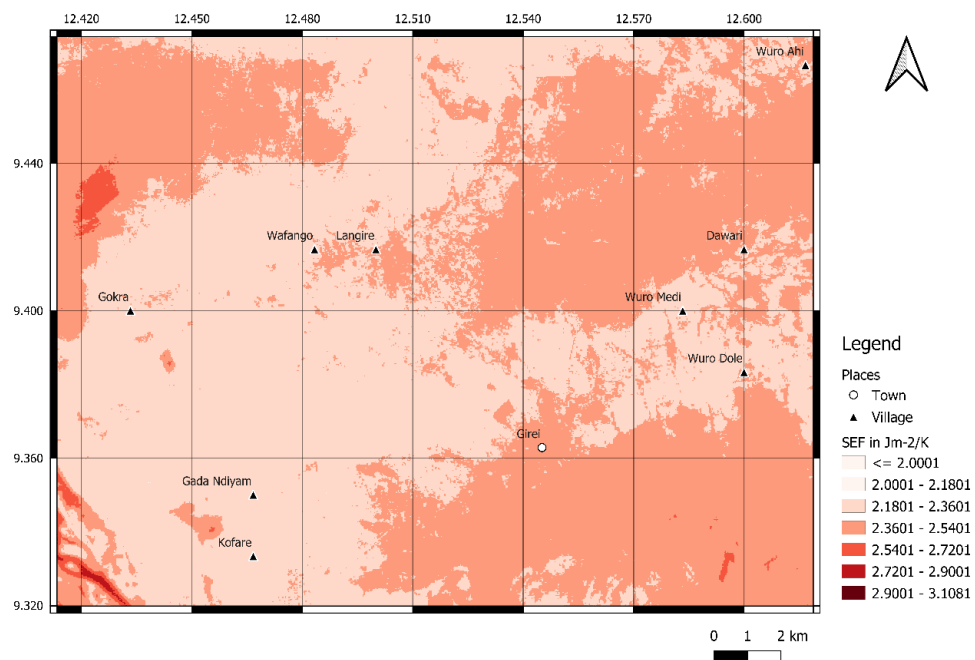**Fig. 11. Dry season (March) 2015 surface entropy flux map of study area (Jm^{-2}K^{-1})**

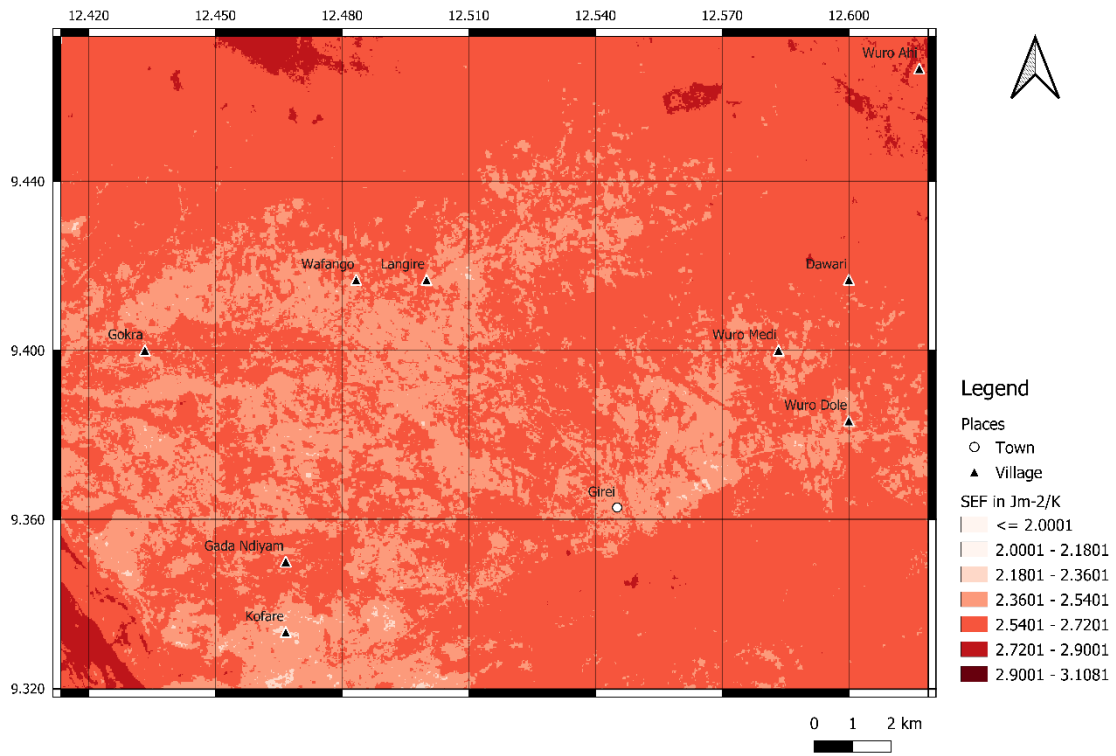**Fig. 12. Dry season (March) 2017 surface entropy flux map of study area (Jm^{-2}K^{-1})**

Fig. 13. Wet season (September) 2013 surface entropy flux map of study area (Jm^{-2}K^{-1})
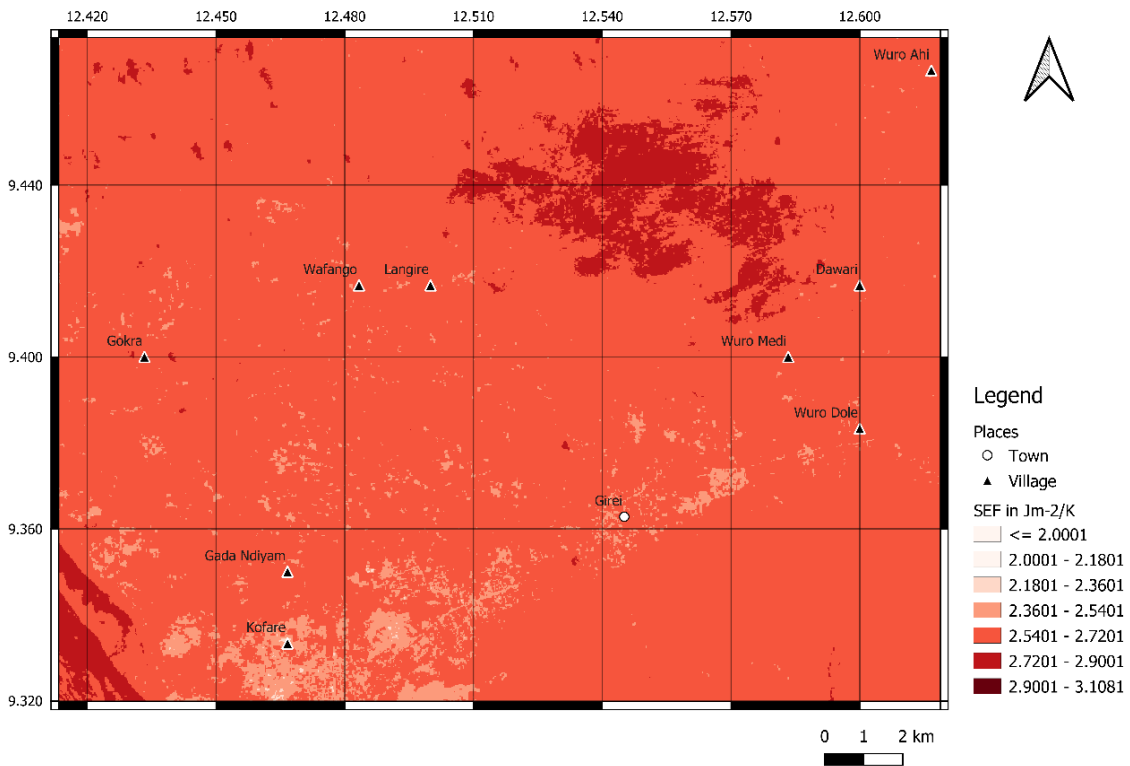

Fig. 14. Wet season (September) 2015 surface entropy flux map of study area (Jm^{-2}K^{-1})
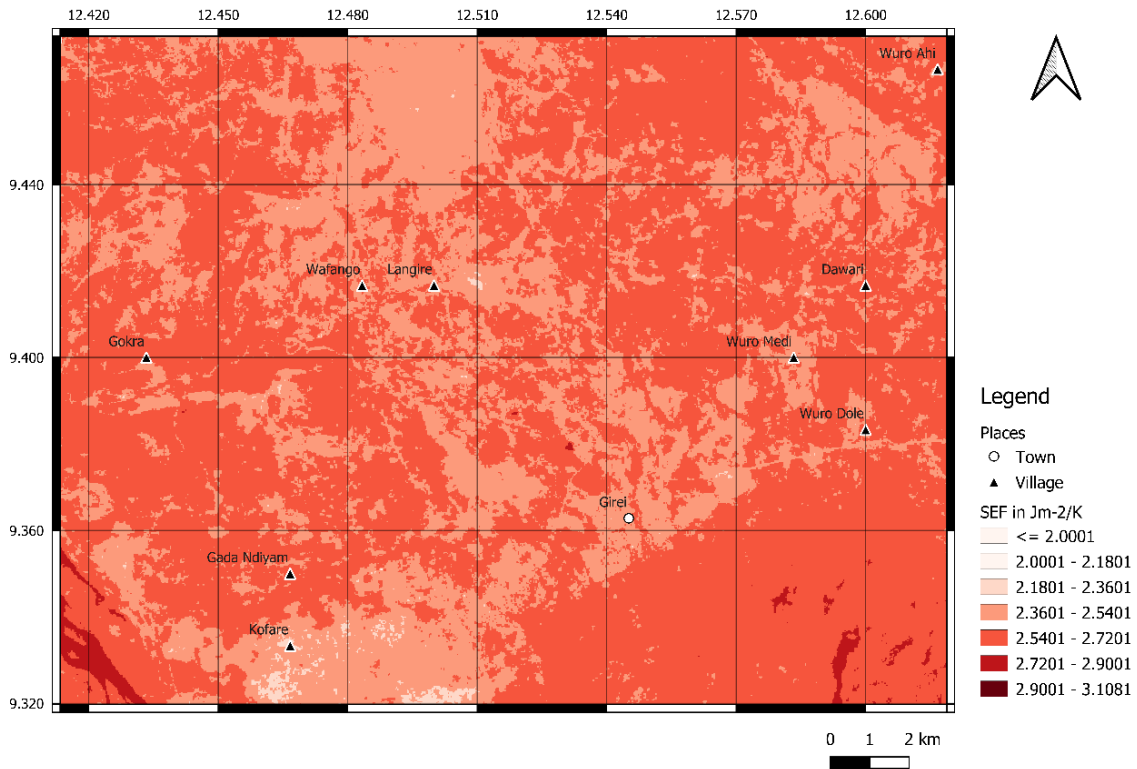
Fig. 15. Wet season (October) 2017 surface entropy flux map of study area (Jm^{-2}K^{-1})

3.4 Relationship between SEF and LST

Regression analysis is about determining how changes in the independent variables are associated with changes in the dependent variable. A regression analysis of the SEF and LST of the study area showed that in the dry season of 2013, about 59.34 % of the variation in SEF was influenced by the variation in LST within a 4.3 % margin of uncertainty. However, in the wet season of the same year, the value increased to about 71.74 %, accounted for by variations in LST within a 3.9 % margin of error. In the dry season of 2015, 92.54 % of the variation in SEF was accounted for by LST variation within a 2.8 % margin of uncertainty. In the wet season of the same year, only 46.67 % of the variation in SEF was influenced by variations in LST within a margin of error of 3.9 %. In the dry season of 2017, it was observed that about 73.16 % of the variation in SEF was influenced by LST within a 3.1 % margin of error. The wet season of the same year was observed to have 86.81 % of the variation in SEF influenced by LST within a margin for error of 3.1 %. These suggests, therefore, that LST has a strong influence on SEF. On the average, LST influences SEF by 75 % in the dry season and 69

% in the wet season, all within 3.5 % margin of error.

The average regression coefficient (R^2) for the dry season of these years is 0.75 while that for the wet season is 0.69. Thus, influence of LST on the variation of SEF within these two seasons, on the average, differ by 6.34 %. Table 8 shows that the level of influence of LST over SEF in the dry season of 2015 was significantly (P = 0.05) greater than that of 2013 by a factor of 1.6. Regardless of the fact that average regression coefficient is higher in the dry seasons, the influence of LST over SEF was generally higher in the wet seasons, except for year 2015. This is attributable to the higher levels of moisture during the season, which translates to high latent energy.

3.5 Relationship between SEF and NDVI

The relationship between SEF and NDVI reveal that only 2.2 % of the variation in SEF was influenced by vegetation within an error margin of 6.7% for the dry season of 2013. The level of influence was higher (11.63 %) during the wet season within a similar (6.8%) error margin. The dry season of 2015 was observed to have 0.9 %

variation in SEF influenced by vegetation within a 10% margin of error, 1.2 % variation within a 5.3 % margin of error in the wet season of same year. Year 2017 dry season show 23.3 % variation in SEF influenced by vegetation within a 5.2 % margin of error whereas the wet season of the year shows 31.9 % variation in SEF influenced by vegetation with a 5.5 % error margin. The low regression coefficient values of the dry season compared to the wet season (Table 10 and 11) as well as the relatively large error margins indicate that vegetation by itself has no influence on the variations in SEF. This suggests that variation in SEF is greatly influenced by moisture rather than vegetation (directly i.e., canopy), given the increased influence during the wet season. Thus, regression analysis between SEF and NDVI reveals that vegetation cover has no appreciable influence on SEF.

3.6 Comparison of Bare Surface and Vegetation Cover SEF

A two-sample t-test was conducted between randomly sampled SEF values from bare surfaces across the three years and vegetation-covered surfaces. This revealed a significant difference between the mean of the two samples at a 5 % significance level. The sample mean for bare surface SEF values was lower at 2.4942 $Jm^{-2}K^{-1}$ than that of vegetation-covered surface at 2.6081 $Jm^{-2}K^{-1}$.

Table 8. Regression between SEF and LST for dry season (March)

	2013	2015	2017
R^2	0.593440	0.925424	0.736625
R^2_{adj}	0.593439	0.925424	0.736624
R^2_{mse}	0.042923	0.027931	0.030717

3.7 SEF for Land Cover Classification

SEF values for vegetative surfaces and water bodies were presented at the upper end of the varying SEF values as 2.618 ± 0.174 $Jm^{-2}K^{-1}$ and 2.766 ± 0.063 $Jm^{-2}K^{-1}$ respectively (Table 12). This information was used to develop land cover classes presented in Table 13. A SEF land cover map of the study area was generated based on this new classification (Fig. 16). It was observed that free water bodies such as the River Benue (lower left quadrant of map) and large streams in

the Bagale hills (lower right quadrant of map) were properly classified. Bare surfaces around the Kaffare settlements were also classified. It was also observed that a larger portion of the built-up areas was at the lower left quadrant of the study. Thus, the overlap between built-up areas and vegetation on one hand, and that between bare surface and free water bodies experienced with NDVI-based classification is non-existent with SEF-based classification (Table 13).

Table 9. Regression between SEF and LST for wet season (September/October)

	2013	2015	2017
R^2	0.717387	0.466719	0.868121
R^2_{adj}	0.717387	0.466718	0.868120
R^2_{mse}	0.038522	0.038645	0.024209

Table 10. Regression between SEF and NDVI for dry season (March)

	2013	2015	2017
R^2	0.022004	0.009247	0.232485
R^2_{adj}	0.022002	0.009245	0.232484
R^2_{mse}	0.066573	0.101805	0.052436

Table 11. Regression between SEF and NDVI for wet season (March)

	2013	2015	2017
R^2	0.116308	0.012534	0.318786
R^2_{adj}	0.116306	0.012532	0.318785
R^2_{mse}	0.068118	0.052587	0.055022

Table 12. Average SEF values for land cover classes of study area

	Vegetation	Built-Up	Bare Surface	Water Bodies
Mean	2.618	2.487	2.388	2.766
STDV	0.174	0.126	0.084	0.063

Table 13. SEF Land cover classification

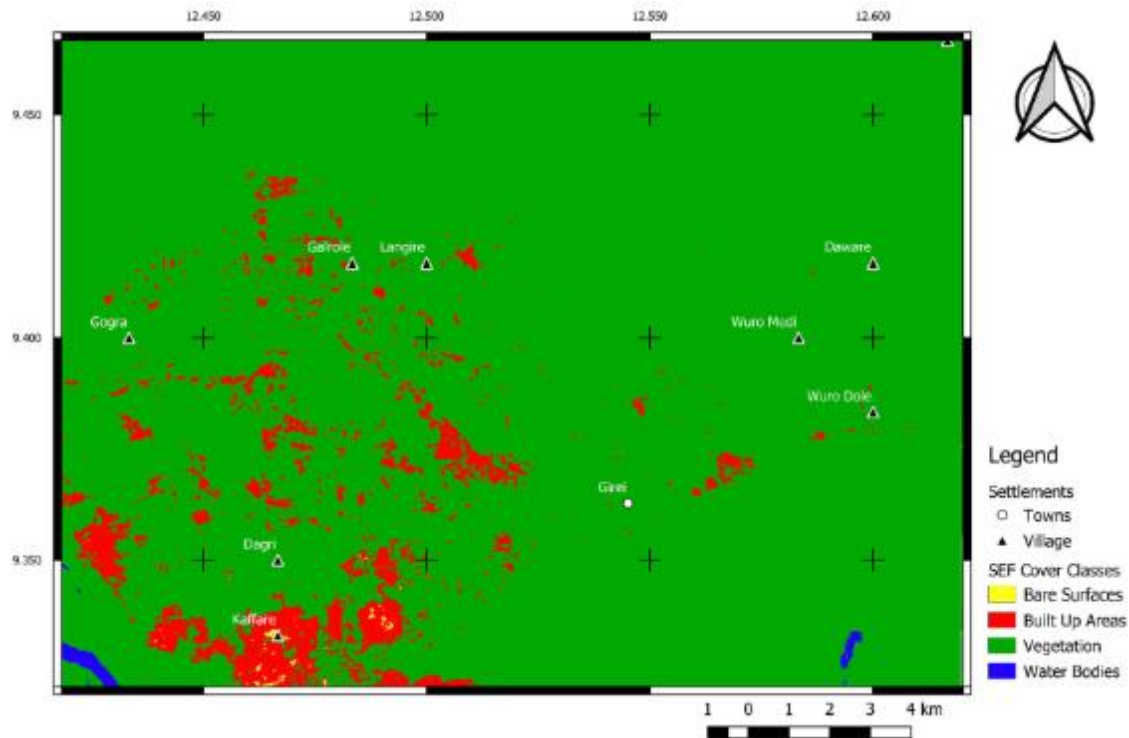|	Boundaries	
	Lower	Upper
Bare Surface	<	2.361
Built-Up	>2.361	2.444
Vegetation	>2.444	2.703
Water	>2.703	>

Fig. 16. SEF reclassified land cover map of study area

4. CONCLUSION

A pragmatic approach was used to measure surface entropy flux (SEF) using the net radiation at the time of satellite overpass and the land surface temperature (LST) of the Landsat 8 data. SEF values successfully distinguished surfaces of free water bodies, built-up areas, vegetation cover and bare surfaces from one another. This result demonstrates that, thermodynamic entropy is a natural metric that could be used for landcover (LC) classification. While LST has considerable influence on SEF, vegetation cover has no appreciable influence on SEF.

COMPETING INTERESTS

Authors have declared that they have no known competing financial interests OR non-financial interests OR personal relationships that could have appeared to influence the work reported in this paper.

REFERENCES

1. Sandlersky R. Krenke A. Solar energy transformation strategies by ecosystems of the Boreal Zone (Thermodynamic analysis based on remote sensing data). *Entropy*, (2020); 22: 1132-

2. Zhong L. Land-atmosphere interactions and their relationships to the Asian monsoon in the Tibetan plateau. (2014). Available: https://doi.org/10.3990/1.9789036536738.

3. Laird NF, Kristovich DAR. Variations of Sensible and Latent Heat Fluxes from a Great Lakes Buoy and Associated Synoptic Weather Patterns. Journal of Hydrometeorology. 2002; 3(1): 3–12.

4. Mallick J, Yogesh K, Bharath BD. Estimation of land surface temperature over Delhi using Landsat-7 ETM+. Journal of Industrial Geophysics Union. 2008;12: 131-140.

5. Hatfield JL, Baker JM, Sauer TJ, Horton R. Soil Heat Flux: Micrometeorology in Agricultural Systems. Agronomy Monograph. 2005; 47: 131–154.

6. Seen DLo, Chehbouni A, Njoku E, Saatchi S, Mougin E, Monteny B. An approach to couple vegetation functioning and soil-vegetation- atmosphere-transfer models for semiarid grasslands during the HAPEX-Sahel experiment. Agricultural and Forest Meteorology. 1997;83(1–2): 49–74.

7. Young NE, Anderson RS, Chignell SM, Vorster AG, Lawrence R, Evangelista PH, A survival guide to Landsat preprocessing. *Ecology*, 2017; 98(4): 920–932.

8. Chavez PS, Image-based atmospheric corrections – revised and improved. Photogrammetric Engineering and Remote Sensing. 1996;62(9): 1025-1036.

9. Wang R, Hou H, Murayama Y, Derdouri A, Spatiotemporal analysis of land use/cover patterns and their relationship with land surface temperature in Nanjing, China. Remote Sensing. 2020;12, 440.

10. Wang R, Gamon JA, Montgomery RA, Townsend PA, Zygielbaum AI, Bitan K, Cavender-Bares J, Seasonal variation in the NDVI-species richness relationship in a prairie grassland experiment (cedar creek). Remote Sensing. 8(2), 2016.

11. Sobrino JA, Jiménez-Muñoz JC, Paolini L, Land surface temperature retrieval from LANDSAT TM 5. Remote Sensing of Environment. 2004; 90(4): 434–440.

12. Cristobal J, Jiménez-Muñoz JC, Sobrino JA, Ninyerola M, Pons X, Improvements in land surface temperature retrieval from the Landsat series thermal band using water vapor and air temperature, Journal of Geophysical Research: Atmosphere. 2009; 114 (D8): 1–16.

13. Agone V Bhamare S, Change detection of vegetation cover Using Remote Sensing and GIS. Journal of Research and Development. 2012. 2(4): 1–12.

14. Bastiaanssen WGM, Regionalization of surface flux densities and moisture indicators in composite terrain: a remote sensing approach under clear skies in Mediterranean climates. Doctoral Thesis, Wageningen Agricultural University, Wageningen the Netherlands.1995; 273.
Available: https://doi.org/90-5485-465-0

15. Finkele K, Jones MB Clifton-Brown J C The surface energy balance. Climate, Weather and Irish Agriculture, 2004; 1: 101–118.

16. Chemin YA, Distributed Benchmarking Framework for Actual ET Models. In: Evapotranspiration - Remote Sensing and Modeling, e-Book (PDF), 2012; 421–436.

17. Saka MG, Jatau DF, Olaniyi WA. Status of Indigenous Tree Species in Girei Forest Reserve. Journal of Research in Forestry, Wildlife and Environment. 2013;5(1):28–40.

18. PVTS. Normalized Difference Vegetation Index (NDVI). 2002;1:1–6. Available:http://www.pvts.net/pdfs/ndvi/3_3 _ndvi.PDF

19. Thornfield F, Hecheltjen A, Menz G, Bi-temporal change detection, change trajectories and time series analysis for forest monitoring. Photogrammetrie-Fernerkundung-Geoinformation. 2015;2: 129–141.

20. Dewidar KH, Rehili BA Assessment of vegetation indices for estimating plant coverage and plant density in the Northern Sarawat Mountains, Saudi Arabia. Merit Research Journal of Agricultural Science and Soil Sciences, 2013. 1(2): 19–32.

21. Pettorelli N, Ryan S, Mueller T, Bunnefeld N; Jedrzejewska B, Lima M, Kausrud K The Normalized Difference Vegetation Index (NDVI): Unforeseen successes in animal ecology. Climate Research, 2011; 46(1):15–27.

22. Webber ME Entropy and the Environment, Mechanical Engineering. 2015; 16.

23. Brunsell NA, Schymanski S J, Kleidon A, Quantifying the thermodynamic entropy budget of the land surface: Is this useful? Earth System Dynamics. 2011;2(1):87–103.

24. Steinborn W, Svirezhev Y, Entropy as an indicator of sustainability in agroecosystems: North Germany Case study. Ecological Modelling. 2000; 133(3): 247–257.